Elasticity, plasticity and fracture toughness at ambient and cryogenic temperatures of epoxy systems used for the impregnation of high-field superconducting magnets

André Brem [a], Barbara J. Gold [a], Bernhard Auchmann [b], Davide Tommasini [b], Theo A. Tervoort [b,*]

[a] *Department of Materials, ETH Zurich, Zurich, Switzerland*
[b] *CERN TE-MPE, Geneva, Switzerland*

ABSTRACT

This study evaluates the thermal expansion coefficient, as well as the elastic-, plastic- and fracture behaviour, at ambient and cryogenic (liquid nitrogen) temperatures, of four different epoxy systems that are used in high-field superconducting magnets, with the emphasis on rate-dependent plasticity as measured by uniaxial compression testing. As expected, both the elastic and plastic behaviour of the epoxy systems at room temperature depend strongly on their distance to the glass transition temperature, but become similar at cryogenic temperature. The rate dependency of the yield stress at room temperature of the four epoxy systems was similar and is well described by the Eyring model. At cryogenic temperatures the rate dependency disappears and the yield stress of all four epoxy systems approach a similar athermal value. The fracture toughness remained equal or even increased upon cooling to cryogenic temperatures for each of the four epoxies. However, the fracture toughness values of the four epoxies tested were quite different from each other, suggesting that fracture toughness not only depends on the van der Waals interactions between the segments but is also determined by other molecular characteristics, such as the network structure.

The emergence of new generations of superconducting magnets in high-energy physics applications have intensified the search for improved epoxy systems to be used as encapsulating materials at cryogenic temperatures [1,2]. The prime function of these epoxy systems is to provide electrical insulation, adhesion and mechanical support for the magnet coils that typically contain a highly brittle ceramic phase, and to prevent any energy-release mechanisms that might lead to heating effects, resulting in a loss of the superconductive state [3]. In addition to the requirements of optimal thermo-mechanical properties, these epoxy systems should also exhibit superior radiation resistance and ideally have a long pot life combined with a low viscosity to enable efficient impregnation of the magnetic coils [4].

The main source of thermal events that lead to local heating and the accompanied loss of the super-conductive state, are typically assumed to be fracture events due to the electro-magnetic Lorenz forces as they occur during operation of the magnets at cryogenic temperatures, aided by thermal stresses accumulated during cooling due to the mismatch in thermal expansion coefficients between the epoxy matrix and the coil

material [5,6]. As a result, studies on the mechanical behaviour of epoxy-encapsulating matrix materials typically have focused on tensile testing and fracture-toughness measurements at ambient and cryogenic temperatures [7,8]. However, mechanical loading in superconducting magnet applications of the epoxy matrix occurs not only in tension, but also in compression, during preloading and due to the strong compressive Lorentz forces as they occur for example towards the midplane in a dipole magnet during operation. In addition, uniaxial compression loading allows to interrogate the yield behaviour of brittle materials, even at cryogenic temperatures, as materials in compression loading are substantially less sensitive to crack propagation [9–11]. It is, therefore, the objective of this study to examine and compare four selected epoxy systems that are used as matrix material in superconductive magnets for their processing windows as determined by their curing kinetics and for their elastic, plastic and fracture behaviour at ambient and cryogenic (liquid nitrogen) temperatures, with emphasis on their rate-dependent plastic deformation as revealed by uniaxial compression measurements. Finally, the data will be used to predict the behaviour of the

epoxy systems in a thermal shock experiment.

1. Materials and methods

1.1. Materials

The four epoxy systems characterized in this study are either commercial products or specifically developed systems by high magnetic field laboratories themselves. When referring to a particular epoxy system, always the whole system comprising resin, hardener and accelerator (if present) is meant, with the exact composition of the individual systems given in Table 1. For some systems, multiple curing procedures can be given, their specific labeling and temperature program is indicated in Tables 1–3, with special emphasis on the exact temperature program, as variation in curing can lead to differences in the final product.

CTD101-K This epoxy system is a product of Composite Technology Development Inc., and is composed of a Bisphenol A diglycidyl ether (DGEBA) based resin (Part A), a hardener of the anhydride type (Part B) and an accelerator of unknown chemical nature (Part C) [12]. The initial preparation is performed as suggested by the supplier and the corresponding mixing ratio is given in Table 1. Part A, which is solid at room temperature, is heated in a round bottom flask to 60 °C for 60 min until it becomes a low viscous fluid. While keeping the temperature between 40 °C to 60 °C, under continuous stirring, Part B and Part C are added. Subsequently, while stirring, the mixture is degassed with a vacuum around 20 mbar to 30 mbar for 20 min to 30 min until bubbles evolve infrequently.

MY750 This epoxy system is a product of Huntsman. The system consists of a liquid, unmodified, solvent-free Bisphenol A resin (Araldite® MY750) and an aliphatic polyamine hardener (Aradur® HY5922). The initial preparation is performed as suggested by the supplier and the corresponding mixing ratio is given in Table 1. The resin Araldite® MY750 is heated in round bottom flask to 40 °C before adding the hardener Aradur® HY5922 under continuous stirring. After this, the temperature is lowered to 30 °C. While stirring, the mixture is degassed with a vacuum around 20 mbar to 30 mbar for 15 min to 30 min until bubbles evolve infrequently.

Mix61 This epoxy system also known as NHMFL 61 and is a proprietary formulation of the National High-Magnetic Field Laboratory (NHMFL, USA, Florida) [13,14]. It is composed of a Bisphenol A diglycidyl ether based resin (Part I), a hardener of the amine type (Part II), a high molecular weight co-reactant of the amine type (Part III) and a liquid low molecular weight additive (Part IV).

The individual constituents were preheated to 60 °C and mixed together in a round bottom flask at 60 °C under continuous stirring for 10 min. The mixture is degassed under continuous stirring with a vacuum around 20 mbar to 30 mbar for 15 min to 30 min until bubbles evolve infrequently.

Table 1

Summary of the non-proprietary formulation details (name and amount in parts by weight (pbw) of the components) of the epoxy systems used in this study.

CTD101-K	pbw	MY750	pbw	MSUT-Twente	pbw
Part A	100	Araldite® MY750	100	Araldite® MY740	100
Part B	90	Aradur® HY5922	55	Aradur® HY906	90
Part C	1.5			Accelerator DY062	0.2

Table 2

Main curing procedures of the four systems for mechanical testing.

CTD101K	MY750	Mix61	MSUT-Twente
110 °C for 5 h	40 °C for 6 h	60 °C for 16 h	85 °C for 4 h
125 °C for 16 h	80 °C for 3 h	100 °C for 24 h	110 °C for 16 h

Table 3

Four different curing procedures for the **CTD101-K** system as suggested by the supplier. The **110–125** profile was applied to samples for mechanical testing.

110–125	110–135	80–135	135
110 °C for 5 h	110 °C for 5 h	80°C for 24 h	135 °C for 1.5 h
125 °C for 16 h	135 °C for 1.5 h	135 °C for 1.5 h	

MSUT-Twente This epoxy system was formulated at the University of Twente in 1986 for the purpose of impregnating high-field magnets. The system consists of a liquid, unmodified, solvent-free Bisphenol A resin (Araldite® MY740), a low-viscosity anhydride hardener (Aradur® HY609), described as methyl 4-endomethylene-tetrahydrophthalic anhydride (nadic methyl anhydride) and benzyl dimethyl amine (BDMA) as accelerator under the name of DY062. The preparation is performed according to the original recipe by the University of Twente with supplemented information from Huntsman. The corresponding mixing ratio is given in Table 1. The resin is heated to 40 °C and the hardener to 45 °C. The accelerator is added to the hardener under continuous stirring for 20 min, then the resin is added. The mixture is continuously stirred for 10 min at 45 °C. The mixture is degassed under continuous stirring with a vacuum of around 40 mbar to 50 mbar for around 20 min to 30 min until bubbles evolve infrequently.

1.2. Curing

For mechanical testing, the four epoxy systems with the curing procedures listed in Table 2, have been cast into plates of 3 mm, 6 mm and 10 mm thickness. The plates were produced by the Epoxy Laboratory at CERN (Geneva, Switzerland) and at the Paul Scherrer Institute (PSI, Villigen, Switzerland) in accordance to the above given mixing and curing procedures. Casting was performed in specially designed moulds, which include an elaborate heating system for precise temperature control and which are connected to vacuum pumps to guarantee a defect-free (bubble-free) cast. After curing, the moulds were not actively cooled to avoid the introduction of thermal stresses. Finally, the required test specimens for the different mechanical tests were cut by high-pressure water-jet cutting at an external company. Sample preparation using water-jet cutting was found to reduce premature damage to samples to a minimum.

Other curing procedures as given in Table 3 for CTD101-K, have been performed in-house. The resin was cast into a silicon template between to thick aluminium plates. The template already had cavities in the required sample shape for testing, hence, no post processing prior to testing was necessary. Curing was performed in a forced convection oven which ensured a homogeneous temperature. Two K-type thermocouples were placed in the mould to monitor the temperature during curing.

1.3. Dynamic viscosity

Viscosity measurements of the degassed and ready-to-use mixtures of epoxy systems have been conducted by means of stress-controlled small-amplitude oscillatory shear (SAOS) experiments at a frequency of 10 rad

s^{-1} and a stress amplitude of 0.75 Pa. The measurements were performed under constant temperature. Depending on the system, different temperature programs were used. In general, experimental temperatures were from 20 °C to 60 °C with steps of 10 °C. Measurements were performed with an MCR302 (Anton Paar, Austria) using a parallel-plate geometry of 25 mm diameter on top and a 25 mm diameter bottom plate attached. A homogeneous temperature distribution over the whole sample was ensured by using a peltier heating plate at the bottom and a peltier heating hood with a nitrogen flow of 3 l min^{-1}. The measuring gap was between 0.4 mm to 0.6 mm. The time elapsed between the end of preparation and the start of the SAOS experiments (transfer to the rheometer and sample loading) was 10 min to 15 min.

1.4. Differential scanning calorimetry (DSC)

All calorimetric measurements were performed using a heat-flux DSC (Mettler-Toledo, 822e). Indium and Zinc standards were used to perform the automated temperature, heat-flow, and tau-lag calibrations. The experiments were performed with a nitrogen flow of 100 ml min^{-1}.

To access the glass-transition temperature T_g and to verify the completeness of the standard curing procedures, DSC measurements were performed. All heating and cooling measurements were performed with a rate of 5 °C min^{-1}. For a baseline calibration of the heat-flow signal, a blank run with an empty pan was performed before the sample measurements. For CTD-101 K and Mix61, temperature cycles from 20 ° C to 200 °C were used, while MY750 and MSUT-Twente were measured from −20 ° C to 200 ° C due to their lower T_g. Samples were directly taken from the inner part of the cured plates for the standard curing procedures given in Table 2 and additional profiles given in Table 3.

1.5. Dynamic mechanical thermal analysis (DMTA)

DMTA measurements were performed using a Mettler Toledo DMA/SDTA861e system equipped with an intra cooler, and a TA Instruments Ares G2 in combination with a forced convection oven and liquid-nitrogen cooling unit. Rectangular shaped bars of around 62 mm × 5.4 mm x 3 mm were analyzed over a support span of 40 mm in 3-point bending mode. A heating and cooling rate of 1 °C min^{-1} between −150 °C and 200 °C was used. For all measurements, a frequency of 1 Hz and an oscillation amplitude of 40 μm (≈ 0.05 % strain) together with a preload of 0.1 N was applied. The machine compliance was taken into account by calibration before the measurements.

1.6. Compression testing

Compression tests at room temperature were performed with a constant cross-head speed on cylindrical samples of around 6 mm in height and 6 mm in diameter using a Zwick Z202 tensile tester equipped with a 20 kN load cell. To avoid any friction between the sample surfaces and the compression plates, a thin film of PTFE oil was spread on the compression plates.

Compression tests at −196 °C were performed in a container filled with liquid nitrogen (see Fig. 1). The home-build setup consists of a double walled stainless-steel vessel with a massive bottom plate for high mechanical stability. To provide good insulating properties, the setup is additionally covered with a 3 cm styrofoam isolation including a proper lid. The thermally isolated container was positioned on the bottom plate of the opened compression setup and centered carefully. Afterwards, the cylindrical samples were placed in the center of the bottom plate and the upper plate was slowly lowered until contact with the sample was reached. To avoid any loss of contact between sample and plates due to shrinking while cooling, a constant load of 20 N was applied to the sample. Subsequently, the container was filled with liquid nitrogen below the rim and the lid was closed. In accordance to the cooling protocol given in the support information, the vessel was re-filled every 2.5 h to keep all components fully immersed in liquid nitrogen to provide a complete cool-down of all components of the setup before the compression measurement was started using a preload of 20 N. Instead of PTFE oil, a polytetrafluoroethylene (PTFE) foil with a thickness of 0.1 mm was placed between the specimen surface and the compression plates of the testing stage. As with the room-temperature compression measurements, the condition of homogeneous, friction-less compression was verified by stopping the measurements before sample failure and to visually inspect the samples to make sure no buckling or barreling was observed. The run-in effect upon initial loading for the cryogenic experiments (see Fig. 9) is due to small non-reproducible misalignment errors (≈ 80 μm).

1.7. Fracture toughness testing

The fracture toughness K_{Ic} was measured by the means of a single-edge notch bending (SENB) test according to ASTM D5045-14. Specimen with width, $W = 10$ mm, thickness $B = 5$mm and support span, $S = 40$ mm were cut from a 10 mm plate together with a 300 μm wide pre-notch of $0.4B$. Pre-cracking was done by tapping a razor blade further into the pre-notch to a depth of 2.5 mm ± 0.25 mm with the method described by Kuppusamy and Tomlinson [15]. The final pre-crack size a consisting of the pre-machined notch and the pre-crack itself was determined subsequent to the measurements using an optical microscope.

All tests were conducted using an Instron 5864 universal testing machine equipped with a 2 kN load cell. Testing speed was set to 1 mm min^{-1} while the testing temperature corresponded to the ambient temperature of around 20 °C. At least five samples with comparable pre-cracks were tested for each epoxy system to ensure reproducibility.

Tests at −196 °C are performed in the setup shown in Fig. 1 (left). The setup allows to determine the load at fracture, but has restrictions on an accurate displacement measurement. This is due to thermal contraction of the PEEK bar (a) and small deviations in alignment between measurement which affect the actual compliance.
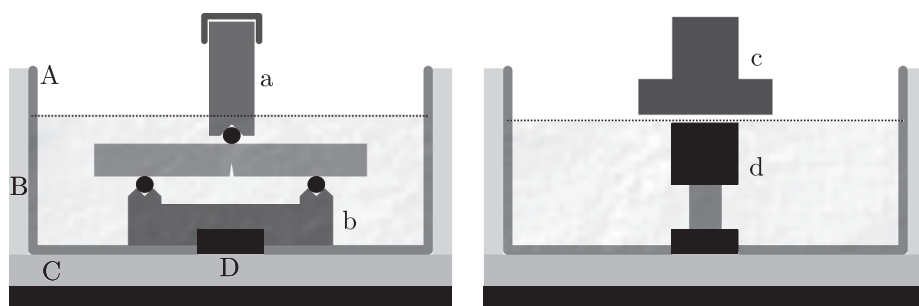

Fig. 1. Schematic of the setup used for cryogenic testing, the dotted line indicates the ideal liquid nitrogen filling level. **A** - rectangular aluminum bowl with a 20 mm concentric hole in the bottom plate, **B** - styrofoam isolation, **C** - flat sandstone plate isolation on top of compression tool bottom plate (black), **D** - stainless steel cylinder of 20 mm fitted into the concentric hole of the aluminium bowl. **a** - notched PEEK slab of 20 mm diameter with a 6 mm diameter steel pin, **b** - aluminium sample holder with two notches supporting 6 mm - diameter steel pins (set apart by support span), the sample holder is placed on a flat 20 mm steel cylinder (black), **c** - upper compression tool plate, **d** - stainless steel cylinder of 20 mm centered on top of the sample.

1.8. Tensile testing

Uniaxial tensile tests with a rate of 0.01 s^{-1} at room temperature were performed on a Zwick Z202 with pneumatic clamps and a 20 kN load cell. Testing was performed according to ISO 527 with a 1AB test geometry. The dogbones had a gauge length of 27 mm and 4 mm x 6 mm cross section. Proper clamping was ensured with 2 bar clamping pressure and 120 grid sandpaper glued to the grippers surface.

1.9. Thermal expansion measurements

Thermal expansion coefficient measurements were performed using a TA Instruments Ares G2 in combination with a forced convection oven and liquid-nitrogen cooling unit. The thermal contraction of rectangular shaped bars of 40 mm x 5.4 mm x 3 mm was measured between a cone-plate geometry. The bar was placed upright between the geometry with the plate at the bottom and the cone on top. A constant load of 0.5 N was applied to hold the sample in place during the measurement. Measurements were started at room temperature and the cooling rate was 1 °C min^{-1}. The thermal contraction of the setup was calibrated by measuring an aluminium bar, with known thermal-expansion coefficient, which had the same length (40 mm) as the epoxy samples.

2. Results and discussion

2.1. Processing

The processing window for the epoxy systems is given by the type and size of the magnet as well as the method of infiltration. For vacuum impregnation, the viscosity of the epoxy system should remain below a given critical value, defined in this study as 1000 Pa s and preferably below 300 Pa s for a minimal time of 250 s. In Fig. 2, the evolution of the dynamic viscosity η_d (the absolute value of the complex viscosity η^*, $\eta_d =$

$|\eta^*|$) shows that for all systems under investigation, processing is possible, as the viscosity remains long enough below the critical value. Only in the case of MY750 epoxy, the viscosity exceeds the critical value a little too soon, which may restrict its use to certain magnet designs or would require a change of the infiltration method like, for example, pressure impregnation.

2.2. Curing

DSC measurements serve as a standard technique to measure the extent of curing. If unreacted functional groups are present, an exothermic peak can be observed when the temperature exceeds T_g or the initial curing temperature. In Fig. 3 no exothermal peaks are present for all of the four samples, which indicates complete curing under the given procedures. However, it should be noted that the absence of an exothermic peak is not equivalent to full conversion. Unreacted functional groups have to be in close proximity to react, so if they are immobilised and/or too far away from each other, no cross-linking reaction will take place. The peak in the signal of the MY750 system directly after the glass transition at 40 °C to 60 °C is ascribed to enthalpy relaxation. The glass transition, T_g, determined by DSC, of all for systems is listed in Table 4.

In case of the CTD101K system there are multiple curing protocols besides the one chosen for this study (see Table 3). DSC measurements after different curing cycles for the CTD101K system are shown in Fig. 4. For the "fastest" curing at 135 °C for 1.5 h, a hint of an exothermic peak emerges, indicative of unreacted functional groups, which is further confirmed by two subsequent DMTA runs as shown in Fig. 5, where T_g has increased in the second run due to post curing during the first run. The other three curing cycles appear to lead to a cured system but with variations in T_g.

The differences in the glass transition temperature, T_g, relate to different degrees of conversion [16–19]. An example of an expression
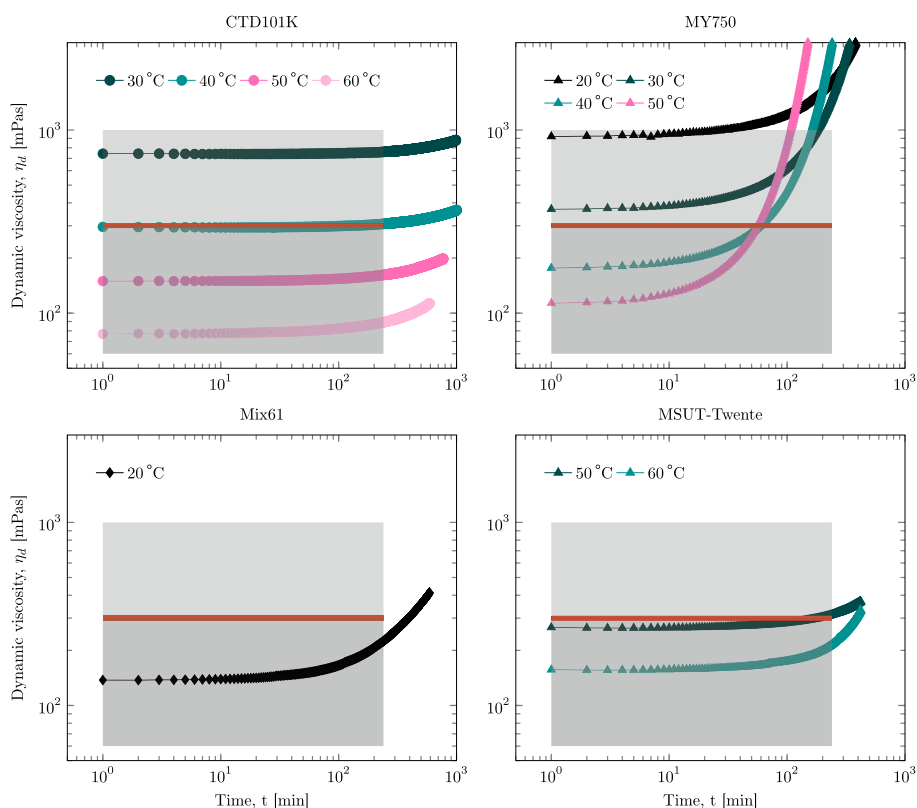

Fig. 2. Progression of the viscosity of the epoxy systems after mixing at various temperatures. The processing window, up to 4 h, is marked in grey and light grey. The red line is at 300 Pa s and marks the processing limit for the initial viscosity.
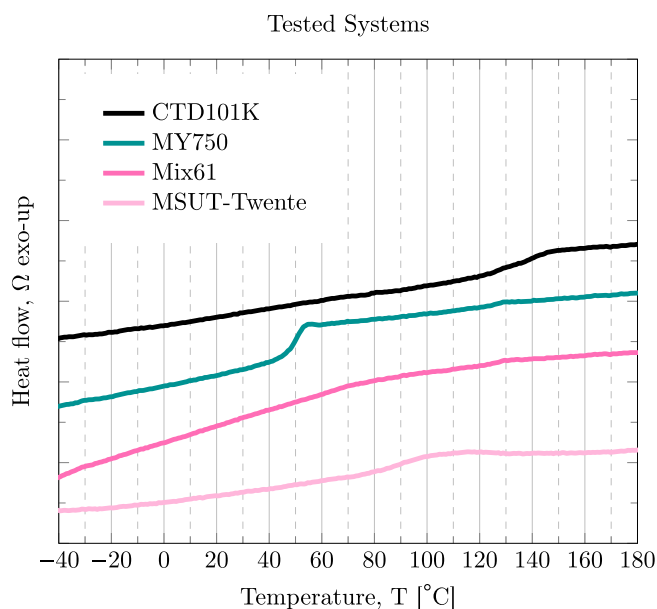
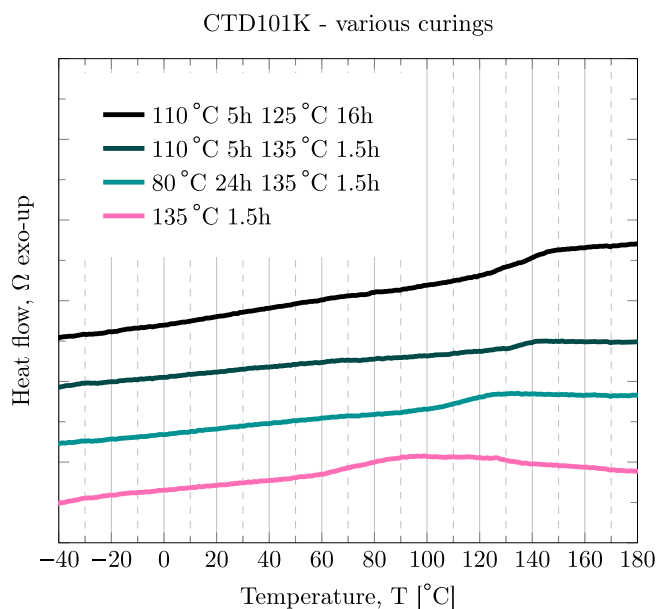**Fig. 3.** First heating signal of samples taken from the cured epoxy systems, the specific curing cycles preceding the measurement are indicated in Table 2. The heating rate is 10 °C min⁻¹.

Table 4
Glass transition temperature, T_g in °C, of the four epoxy systems determined by DSC and DMTA (δ: peak in loss factor, E'': peak in loss modulus).

Technique	CTD101K	MY750	Mix61	MSUT-Twente
DSC - onset	124	45	NA	76
DSC - midpoint	137	49	NA	88
DSC - endset	148	53	NA	97
DMTA $\tan(\delta)_{max}$	145	57	73	82
DMTA E''_{max}	135	51	-20	66

NA: *not available*

Fig. 4. First heating signal of samples taken from the cured CTD101K epoxy system, the specific curing cycles preceding the measurement are indicated in the legend. The heating rate is 10 °C min⁻¹. The first curing cycle in the legend is the one applied for mechanical tests.
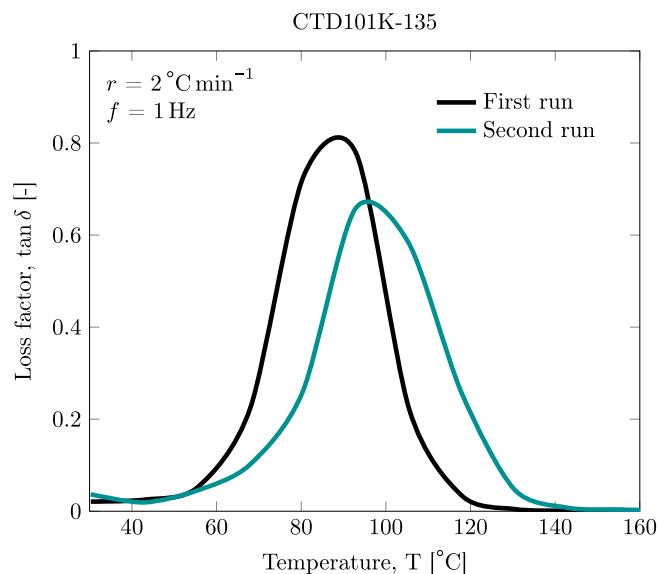

Fig. 5. Two consecutive DMTA measurements from 30 °C to 160 °C of the same sample. In the second run T_g inferred from the peak in tan δ is increased by 10 °C.

that relates T_g with conversion, χ, is given in Eq. (1), with T_{g0} the glass transition of the uncured system, $T_{g\infty}$ of the fully cured system, and $\lambda = \Delta c_{p\infty}/\Delta c_{p0}$, is the ratio of changes in the specific heat through the glass transition for the fully cured and the initial samples [16].

$$\frac{T_g - T_{g0}}{T_{g\infty} - T_{g0}} = \frac{\lambda\chi}{1 - (1 - \lambda)\chi} \tag{1}$$

Based on this, the curing cycle $110 - 125$ (see Table 3), leads to the highest degree of conversion, since the glass transition, as shown in Fig. 6, is the highest for that particular curing cycle.

In Table 4 the glass-transition temperatures are listed based on technique and evaluation method used.

2.3. Mechanical properties

2.3.1. Elasticity

Fig. 7 shows the storage moduli, E' (top) and loss factors, $\tan(\delta)$ (bottom), for all epoxy systems used in this study for temperatures ranging from −160 °C to 20 °C (left) and 35 °C to 200 °C (right). When crossing the glass transition temperature (called the "α-transition"), T_g, during heating, the storage modulus drops by two orders of magnitude. The temperature interval over which the vitrifaction occurs follows from the major peaks in the $\tan(\delta)$ graphs and increases from narrow (16 °C full width at half maximum (FWHM) to wide (40 °C FWHM) between the different systems in the following order MY750, CTD101K, MSUT-Twente and Mix61.

Far below T_g at −80 °C to −100 °C, all four systems show secondary relaxations (so-called "β-relaxations") identified by local smaller maxima in tanδ. At temperatures below these β-transitions, the loss factors of all epoxy systems become very low, indicating close to pure elastic deformation behaviour where the storage modulus equals the Young's modulus. In Fig. 7 it can be seen that at these low temperatures, the storage moduli (Young's moduli) of all four systems converge to similar values. This can be explained as follows: according to Grüneisens first rule for isotropic van der Waals materials, such as amorphous polymers, at cryogenic temperatures close to zero Kelvin, the bulk modulus K_{0K} and, therewith, the Young's modulus, E_{0K}, can be expressed as a function of the cohesive energy density, E_{coh}, the molar volume at 0 K, V_{0K}, the coefficients of the Lennard-Jones potential for Van-der-Waals interactions, $m = 6$ and $n = 12$, and the Poisson's ratio ν, as [20]:
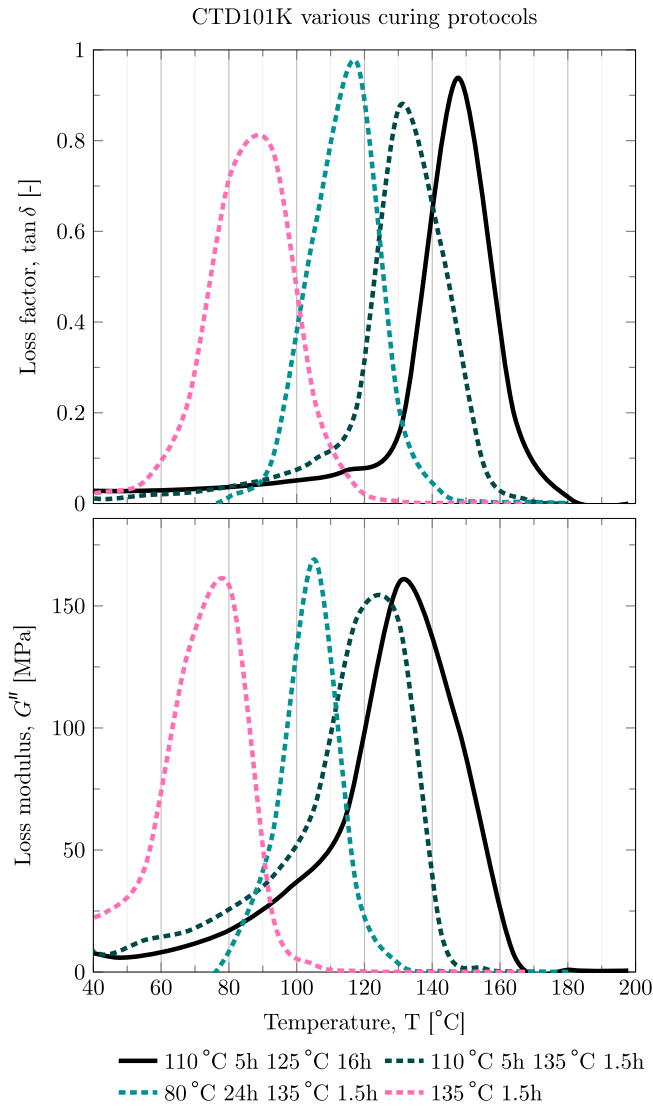
Fig. 6. Loss factor and loss modulus from DMTA measurements of the CTD101K epoxy system after curing under various protocols.

$$E_{0K} = 3(1 - 2\nu)K_{0K} = 3(1 - 2\nu)\frac{mn}{4}\frac{E_{coh}}{V_{0K}} \tag{2}$$

For the different epoxy systems (and polymer systems in general) at cryogenic temperatures, the cohesive energy density, the molar volume and Poison's constant are dominated by the van der Waals forces and, therefore, expected to be similar, from which it follows that the moduli at low temperatures ($T = 0K$) will be roughly equal [21–23]. This is confirmed in Fig. 7, which shows that at a temperature of $T = -160\,°C$, all moduli values converge to about $E_{0K} \approx 6 - 8$ GPa.

2.3.2. Tensile testing

Besides small-amplitude oscillatory shear testing, the samples were also subjected to finite uniaxial tensile deformation (tensile testing). The results are shown in Fig. 8. In this figure, it can be seen that, except for the Mix61 system, all studied epoxies are too brittle to allow for the determination of the tensile yield stress determination. Even though the strain rate applied during the tensile deformation, $\dot{\varepsilon}_0 = 0.001 s^{-1}$ is low compared to the deformation rates in the DMTA experiments performed at 1 Hz, the Young's moduli, determined as the initial slope of the stress–strain curves, are in good agreement with the values as measured with DMTA, except for the Mix61 system. The modulus of Mix61 epoxy

measured with DMTA is higher than the modulus from the stress–strain curve, as the mechanical behaviour of the Mix61 system is strongly strain-rate dependent around room temperature as can be seen in Fig. 7.

In case the fracture toughness is known, the strength values measured in tensile deformation can be used to estimate the flaw size due to water cutting (see Section 3).

2.3.3. Plasticity

For isotropic amorphous polymers at very low temperatures, far below any mechanical transition, the shear-yield stress τ_y is known to approach its theoretical value $\tau_y = \frac{G}{15}$, where G is the low-temperature elastic shear modulus[24–26]. Assuming the applicability of the Von Mises yield criterion, the shear yield stress τ_y is related to the yield stress in uniaxial deformation σ_y as $\sigma_y = \sqrt{3}\tau_y$. As the elastic moduli are converging to similar values at cryogenic temperatures, the same is, therefore, to be expected for the yield stress σ_y. This is indeed observed for the yield stress values σ_y, measured in uniaxial compression to avoid brittle fracture at cryogenic temperatures ($T = -196\,°C$), as shown in Fig. 9, depicting a saturation of the yield stress at a level of around 450 MPa to 500 MPa for all epoxy systems.

At room temperature, the epoxy systems exhibit rate-dependent yielding, as depicted for uniaxial compression in Fig. 10. For polymer systems, this kind of plastic deformation behavior is well described by the Eyring theory [27,28]. In Eyring rate-dependent yielding, it is assumed that at the yield point, where the applied strain rate equals the plastic strain rate, the material behaves as a generalised non-Newtonian liquid. The Eyring constitutive equation for the non-Newtonian viscosity that determines the plastic strain rate as a function of stress, then follows from a stress-dependent increase in molecular mobility and leads to the following relation of the yield stress as a function of the applied strain rate at high stress levels [28]:

$$\sigma_y = \frac{kT}{V^*}\ln\left(\frac{2\dot{\varepsilon}}{\dot{\varepsilon}_0}\right) + \frac{\Delta U}{V^*} \tag{3}$$

Here, k is Boltzmann's constant, V^* is the so-called "activation volume", a material parameter that describes the stress-induced mobility, ΔU is the activation energy and $\dot{\varepsilon}_0$ is another material parameter that is related to the fundamental jump frequency. From Eq. (3) it follows that at constant temperature, a plot of the yield stress as a function of the logarithm of the applied strain rate yields a straight line, the slope of which is related to the activation volume. These so-called Eyring plots for all epoxy systems are shown in Fig. 12. From this figure it is clear that the rate-dependent yield behaviour is well described by the Eyring equation (Eq. (3)), the corresponding values for the activation volumes are listed in Table 5.

According to the Eyring equation, the strain-rate dependence of the yield stress vanishes at cryogenic temperatures ($T = 0K$), where the yield stress adopts the athermal value of $\sigma_y = \Delta U/V^*$. This was indeed observed experimentally as the yield stresses measured in compression (see Fig. 11) did not depict any strain-rate dependence anymore. Finally, it was observed for the Mix61 system, that the yield stress measured at room temperature at a strain rate of $\dot{\varepsilon}_0 = 0.001\,s^{-1}$ in uniaxial tensile ($\sigma_y = 23$ MPa, see Fig. 8) and compression ($\sigma_y = 31$ MPa, see Fig. 10), differed substantially, indicative of a rather strong dependence of the yield stress on the hydrostatic pressure, which has been observed before for epoxy systems that contain a plasticizer [20].

2.3.4. Fracture behaviour

The results of fracture toughness (K_{Ic}) measurements at room temperature and in liquid nitrogen (-196 °C) are shown in Fig. 13. Interestingly, the K_{Ic} values tend to be higher at cryogenic temperatures for all four systems. For the CTD101K epoxy system, K_{Ic} more than doubles at cryogenic temperatures and the MSUT-Twente system shows an increase of 50%. In general, an important contribution to the fracture
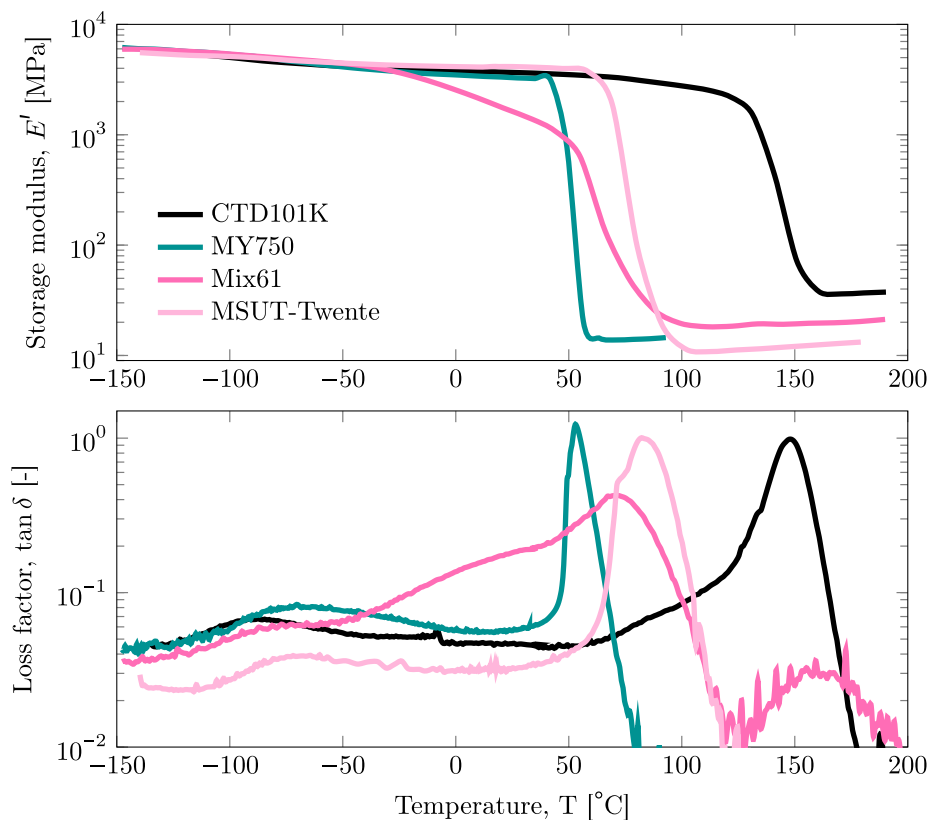
Fig. 7. Storage modulus, E' and loss factor $\tan\delta$ of all epoxy systems measured at 1 Hz as a function of temperature.
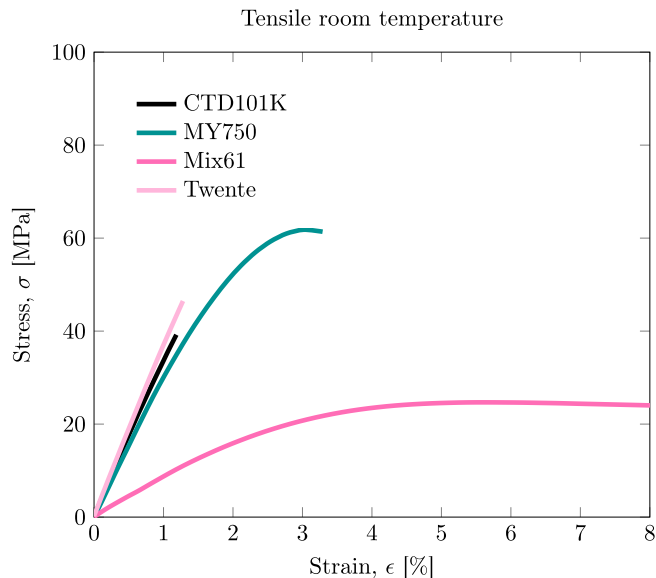

Fig. 8. Uniaxial tensile deformation of all epoxy systems, measured at room temperature and an initial strain rate of $\dot{\varepsilon}_0 = 0.001$ s^{-1}.

toughness of a material is the size of the plastic deformation zone behind a crack tip. However, despite the similar values of the Young's modulus and the yield stress values of all epoxy systems at cryogenic temperatures as determined in this study, substantial differences were measured for the fracture toughness values of the epoxies at these cryogenic temperatures. It, therefore, appears that cryogenic fracture toughness depends (also) on other molecular characteristics such as network structure, that have no direct influence on stiffness or yield stress. For

example, inhomogenous network structures have been found to enhance the fracture toughness at cryogenic [7] and ambient temperatures. [29–31].

Among the four systems, the MY750 exhibits a high value of K_{Ic}. As a comparison to the 4.6 MPa $\sqrt{m}$ of the MY750, polycarbonate, an amorphous polymer well-known for its high toughness, has a K_{Ic} of around 3.2 MPa $\sqrt{m}$ [32].

2.4. Thermal expansion

Also the thermal expansion behaviour of isotropic polymer systems is mainly determined by the van der Waals forces between the polymer segments. As a result, as with the elastic moduli, the thermal expansion coefficients of all epoxy systems at cryogenic temperatures are expected to be of similar value. This is confirmed in Fig. 14. Below −60 °C to −80 °C, the thermal expansion coefficient is identical for all four system with a value of 44 ± 4 × 10^{-6} °C. The steeper slope and kink above and at $T = -40$ °C for the Mix61, coincides with the endset of the drop in the loss factor shown in Fig. 7 (left-bottom).

3. Thermal shock testing

The thermal shock test is a simple experiment where a disk of cured epoxy is tossed into liquid nitrogen to generate thermal stresses, and is often used as a basic screening test for the suitability of an epoxy system in cryogenic applications [8]. To calculate the thermal stresses arising in such a test, frozen-in stresses that occur during polymerization [33] are neglected. Furthermore, it is assumed that the elastic modulus E is temperature independent and that the temperature change is instantaneous. In other words, upon quenching, the surface of the epoxy is assumed to adopt immediately a surface temperature of −196 °C whereas the interior still is at room temperature. With $\Delta\alpha$ the difference in thermal expansion coefficient between the cold surface and the warm
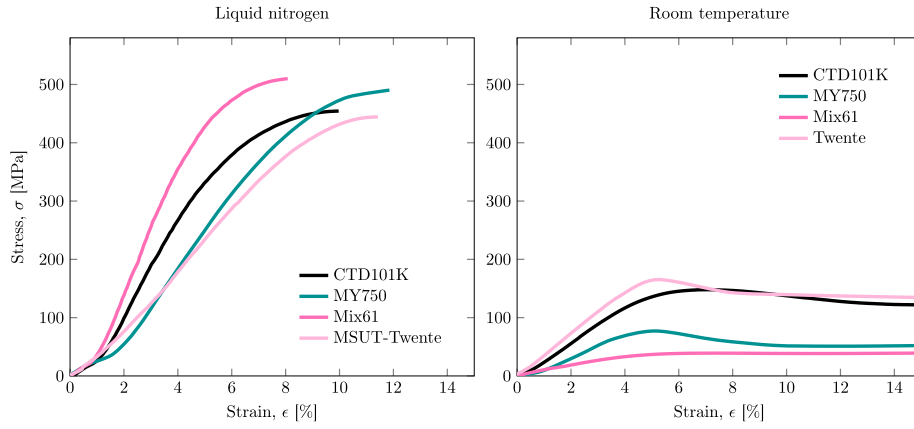
Fig. 9. Comparison between the yield behaviour as measured in uniaxial compression testing of all epoxy systems at liquid nitrogen temperature (left) and room temperature (right) at an initial strain rate of $\dot{\epsilon}_0 = 0.01 \text{ s}^{-1}$. The run-in effect upon initial loading for the cryogenic experiments is due to small non-reproducible misalignment errors ($\approx 80 \text{ μm}$).
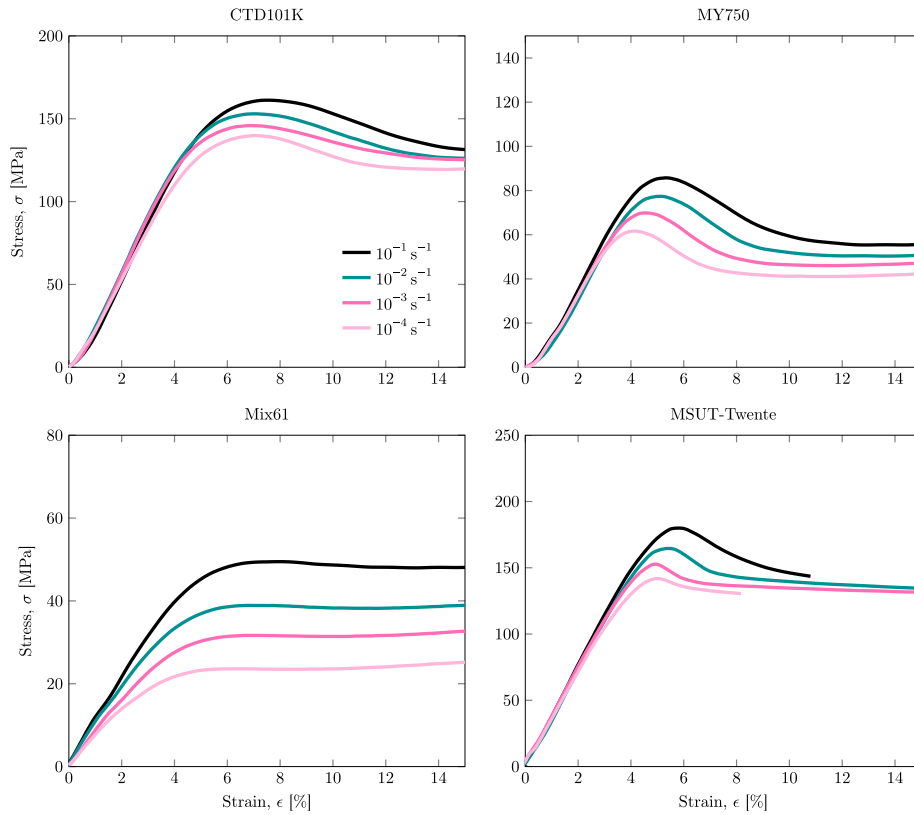

Fig. 10. Rate-dependent plastic deformation behaviour of the four epoxy systems measured at room temperature in uniaxial compression at initial strain rates ranging from $\times 10^{-1}$ to $\times 10^{-4} \text{ s}^{-1}$.

Table 5
Eyring activation volumes for the various epoxy systems as determined from Fig. 12.

	CTD101K	MY750	Mix61	MSUT-Twente
V^* [nm^3]	1.3	1.2	1.1	0.9

bulk material, and ν the Poisson's ratio, the biaxial thermal stress at the surface is then equal to:

$$\sigma_{\text{thermal}} = \frac{E}{(1 - \nu)} * \Delta\alpha\Delta T \tag{4}$$

If the thermal stress reaches the critical fracture stress σ_c, the part will break. The maximum instantaneous temperature change on the surface that the epoxy can withstand, ΔT_{max}, then follows from Eq. (4) as:

$$\Delta T_{\text{max}} = \frac{(1 - \nu)\sigma_c}{E\Delta\alpha} \tag{5}$$

The critical stress σ_c is determined by the fracture toughness K_{Ic} of the epoxy system and the maximum crack length on the surface of a sample:

$$\sigma_c = \frac{K_{Ic}}{\beta\sqrt{\pi c}} \tag{6}$$

Here, c is the crack length and β is a crack-shape factor that is in the
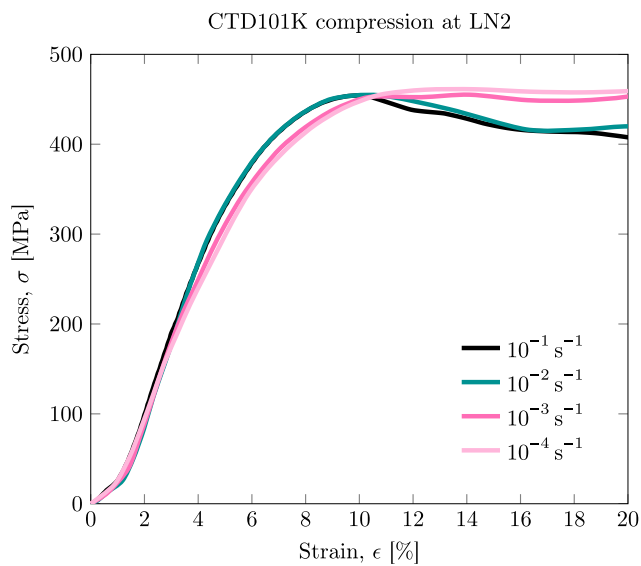
Fig. 11. The yield stress of the CTD101K epoxy system, measured at liquid nitrogen temperature in uniaxial compression, was found to be independent of strain rate for initial strain rates ranging from $\times 10^{-1}$ to $\times 10^{-4}$ s^{-1}. The same behaviour was observed for the other three epoxy systems.
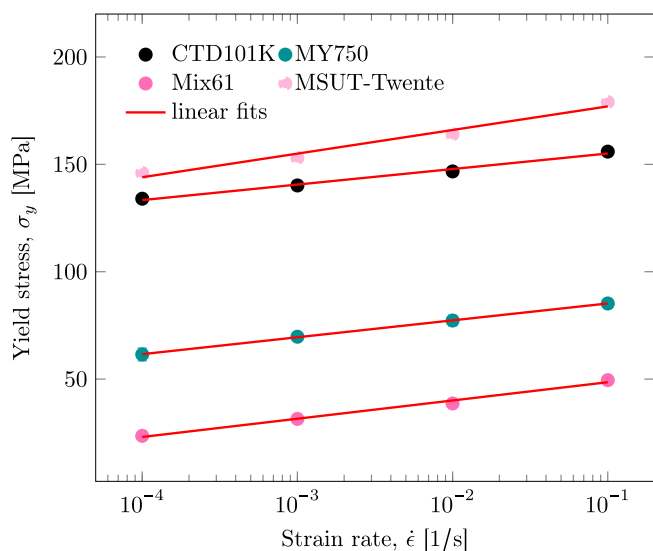

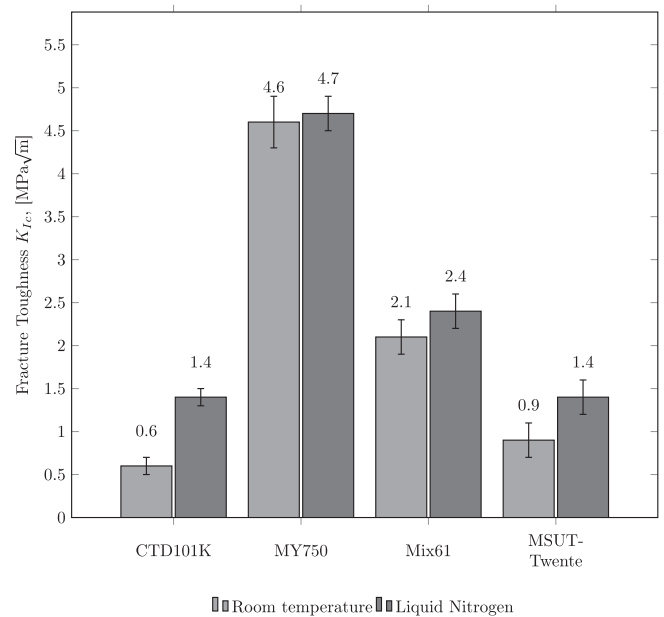**Fig. 12.** Eyring analysis of the yield points from Fig. 10.

Fig. 13. Fracture toughness values for the various epoxy systems measured at room temperature and liquid nitrogen temperature.
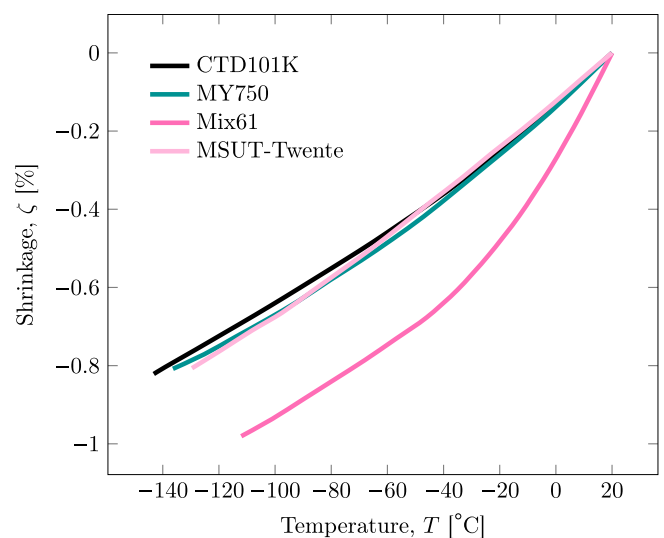

Fig. 14. Thermal contraction as a function of temperature for the various epoxy systems.

order of $\beta = 1.2$ for penny-shaped surface cracks. As all samples were cut by water jet cutting, the surface cracks are assumed to be the same size for all four epoxy systems and were estimated from the strength of the tensile experiments as $c = 75$ μm. This allowed the critical stress to be estimated for each epoxy systems using Eq. (6). Substitution of these σ_c values into Eq. (5) then allowed the calculation of the maximum temperature difference that each of the epoxy systems can withstand. In Table 6 these ΔT_{max} values based on Eq. (5) are listed together with the relevant material parameters. In case of a thermal shock test from room temperature to liquid nitrogen, ΔT equals 216 °C. For the CTD101K and MSUT-Twente system this would exceed the maximum thermal stress the material can withstand without fracture as the calculated ΔT_{max} is below 216 °C for these two systems, whereas this simple model (Eq. (6)) predicts that the Mix61 and MY750 systems would survive this thermal treatment as ΔT_{max} for these two systems is larger than 216 °C.

To verify this outcome experimentally, squares of roughly 30 × 30 mm were cut out from the 3 mm epoxy plates and tossed into liquid

nitrogen. Visual inspection of the samples shown in Fig. 15 indeed showed that the CTD101K and the MSUT-Twente system were cracked.

4. Conclusions

The mechanical and thermal data obtained in this study present an extensive mechanical and thermal characterisation of four epoxy systems, from room temperature down to cryogenic temperatures. From the measured data the following conclusions emerge: at room temperature, both the elastic and plastic deformation behaviour are mainly determined by the distance towards the glass transition temperature and the width of the α-transition. If T_g is close to room temperature and has a broad transition, such as is the case for the Mix61 system, the material is soft and tough. For epoxies with a high glass transition temperature, such as the CTD101K system, the material becomes progressively stiff and brittle at room temperature. Far below the glass transition tem-

Table 6
Thermal shock test.

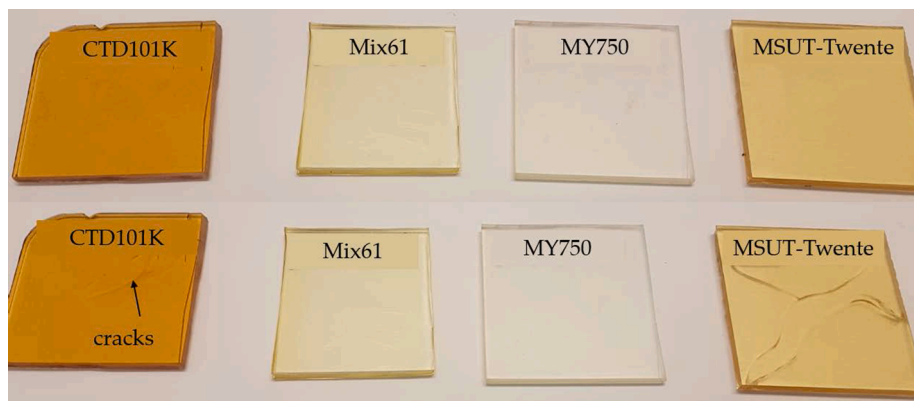| Resin	K_{Ic} exp. MPa$\sqrt{m}$	$c*$ cal. μm	σ_c cal. MPa	E exp. GPa	α exp. $K^{-1} * 10^{-6}$	ν est. -	ΔT_{max} cal. K	
CTD101K	1.4	75	76	6	50	0.3	177	✕
Mix61	2.4	75	130	6.8	50	0.3	268	✓
MY750	4.7	75	255	7	50	0.3	510	✓
MSUT-Twente	1.4	75	76	6.9	50	0.3	154	✕

Fig. 15. Thermal shock experiment performed on the four epoxy systems. The top row shows the samples before and the bottom row after tossing the samples in liquid nitrogen. Both the CTD101K and the MSUT-Twente samples did not survive the thermal shock treatment.

perature, at cryogenic temperatures, for isotropic polymers, such as epoxies, the elastic moduli, the yield stress and thermal expansion co-efficient are all mainly determined by the van der Waals interactions between the polymer segments and are, therefore, similar in magnitude. This is, however, not true for the fracture toughness, which apparently also depends on other molecular characteristics, such as the network structure. The rate dependency of the yield stress at room temperature of the epoxy systems was similar and is well described by the Eyring model. At cryogenic temperatures the rate dependency disappears and the yield stress values of all four epoxy systems approach a similar athermal value.

As superconducting cables and other metallic structural components in a magnet coil have a thermal expansion coefficient that is typically one order of magnitude lower than van der Waals materials like epoxies, it is unavoidable that during cooling thermal stresses will develop, even at low cooling rates. These thermal stresses will start to accumulate upon cooling below T_g, which means that low-T_g systems will tend to have less thermal stress. These thermal stresses in combination with stresses that develop due to the Lorenz forces during operation of the magnet, will initiate cracks, depending on the level of adhesion and on the fracture toughness of the epoxy system in use. The build-up of thermal stresses might be reduced by mixing the epoxy with ceramic or metal fillers, as these filler materials will lower the thermal expansion coefficient of the epoxy-filler composite. This comes, however, often at the expense of a reduction in the fracture toughness and increased viscosity.

A simple model to estimate the maximum temperature difference that a material can withstand during a thermal shock experiment was used to demonstrate the usefulness of the material data determined in this work.

CRediT authorship contribution statement

André Brem: Conceptualization, Investigation, Writing - original draft. **Barbara J. Gold:** Investigation. **Bernhard Auchmann:** Conceptualization, Supervision, Funding acquisition. **Davide Tommasini:** Conceptualization, Project administration, Funding acquisition. **Theo A. Tervoort:** Conceptualization, Methodology, Supervision, Writing - review & editing, Funding acquisition.

Declaration of Competing Interest

The authors declare that they have no known competing financial interests or personal relationships that could have appeared to influence the work reported in this paper.

Acknowledgements

References

[1] Yang JP, Chen ZK, Yang G, Fu SY, Ye L. Simultaneous improvements in the cryogenic tensile strength, ductility and impact strength of epoxy resins by a hyperbranched polymer. Polymer 2008;49(13–14):3168–75.

[2] Chen ZK, Yang G, Yang JP, Fu SY, Ye L, Huang YG. Simultaneously increasing cryogenic strength, ductility and impact resistance of epoxy resins modified by n-butyl glycidyl ether. Polymer 2009;50(5):1316–23.

[3] Iwasa Y. Experimental and theoretical investigation of mechanical disturbances in epoxy-impregnated superconducting coils. 1. General introduction. Cryogenics 1985;25(6):304–6.

[4] Evans D, Morgan JT, Stapleton GB. Epoxy resins for superconducting magnet encapsulation. Tech rep, Chemical Technology Group, Rutherford High Energy Laboratory; 1972.

[5] Tsukamoto O, Maguire JF, Bobrov ES, Iwasa Y. Identification of quench origins in a superconductor with acoustic emission and voltage measurements. Appl Phys Lett 1981;39(2):172–4.

[6] Bobrov ES, Williams JE, Iwasa Y. Experimental and theoretical investigation of mechanical disturbances in epoxy-impregnated superconducting coils. 2. Shear-

stress-induced epoxy fracture as the principal source of premature quenches and training theoretical analysis. Cryogenics 1985;25(6):307–16.

[7] Ueki T, Nishijima S, Izumi Y. Designing of epoxy resin systems for cryogenic use. Cryogenics 2005;45(2):141–8.

[8] Yin S, Arbelaez D, Swanson J, Shen T. Epoxy resins for vacuum impregnating superconducting magnets: A review and tests of key properties. IEEE Trans Appl Superconduct, 29 (5).

[9] Govaert LE, Timmermans PHM, Brekelmans WAM. The influence of intrinsic strain softening on strain localization in polycarbonate: Modeling and experimental validation. J Eng Mater Technol-Trans ASME 2000;122(2):177–85.

[10] Gold B, Auchmann B, Tommasini D, Tervoort TA. Tough epoxy systems for the impregnation of high field superconducting magnets. in: presented at the Int. Cryogenic Mater. Conf., Hartford; 2019.

[11] Yin S, Swanson J, Shen T. Design of a high toughness epoxy for superconducting magnets and its key properties. IEEE Trans Appl Supercond, 30 (4).

[12] Fabian PE. Highly radiation-resistant vacuum impregnation resin systems for fusion magnet insulation 2003;295 (May 2002) 295–304.

[13] Brennan AB, Miller TM, Arnold JJ, Huang KV, Gephart NL, Markewicz WD. Thermomechanical properties of a toughened epoxy for impregnating superconducting magnets. Cryogenics 1995;35(11):783–5.

[14] Markiewicz WD, Dixon IR, Dougherty JL, Pickard KW, Brennan AB. Properties of epoxy NHMFL 61 for superconducting magnet impregnation. in: Preprint of ICMC/CEC 1997, Portland, Oregon; 1997.

[15] Kuppusamy N, Tomlinson RA. Repeatable pre-cracking preparation for fracture testing of polymeric materials. Eng Fract Mech 2016;152:81–7.

[16] Pascault JP, Williams RJJ. Glass transition temperature versus conversion relationships for thermosetting polymers. J Polym Sci, Part B: Polym Phys 1990;28 (1):85–95.

[17] Hale A, Macosko CW, Bair HE. Glass transition temperature as a function of conversion in thermosetting polymers. Macromolecules 1991;24(9):2610–21.

[18] Simon SL, Gillham JK. Reaction kinetics and ttt cure diagrams for off-stoichiometric ratios of a high-tg epoxy/amine system. J Appl Polym Sci 1992;46 (7):1245–70.

[19] Ogata M, Kinjo N, Kawata T. Effects of crosslinking on physical properties of phenol–formaldehyde novolac cured epoxy resins. J Appl Polym Sci 1993;48(4): 583–601.

[20] Broadhurst MG. Bulk modulus and grüneisen parameters for linear polymers. J Chem Phys 1970;52(7):3634–41.

[21] Foreman JP, Porter D, Behzadi S, Jones FR. A model for the prediction of structure–property relations in cross-linked polymers. Polymer 2008;49(25): 5588–95.

[22] Foreman JP, Porter D, Behzadi S, Curtis PT, Jones FR. Predicting the thermomechanical properties of an epoxy resin blend as a function of temperature and strain rate. Compos Part A: Appl Sci Manuf 2010;41(9):1072–6.

[23] Li C, Strachan A. Cohesive energy density and solubility parameter evolution during the curing of thermoset. Polymer 2018;135:162–70.

[24] MacMillan NH. The theoretical strength of solids. J Mater Sci 1972;7(2):239–54.

[25] Argon AS. A theory for the low-temperature plastic deformation of glassy polymers. Phil Mag 1973;28(4):839–65.

[26] Seitz JT. The estimation of mechanical properties of polymers from molecular structure. J Appl Polym Sci 1993;49(8):1331–51.

[27] Eyring H. Viscosity, plasticity, and diffusion as examples of absolute reaction rates. J Chem Phys 1936;4(4):283–91.

[28] Govaert LE, van der Vegt AK, van Drongelen M. Polymers, from Structures to Properties. Delft, the Netherlands: Delft Academic Press; 2019.

[29] Sahagun CM, Morgan SE. Thermal control of nanostructure and molecular network development in epoxy-amine thermosets. ACS Appl Mater Interfaces 2012;4(2): 564–72. https://doi.org/10.1021/am201515y.

[30] Sharifi M, Jang CW, Abrams CF, Palmese GR. Toughened epoxy polymers via rearrangement of network topology. J Mater Chem A 2014;2(38):16071–82. https://doi.org/10.1039/c4ta03051f.

[31] Aoki M, Shundo A, Yamamoto S, Tanaka K. Effect of a heterogeneous network on glass transition dynamics and solvent crack behavior of epoxy resins. Soft Matter 2020;16(32):7470–8. https://doi.org/10.1039/D0SM00625D.

[32] Hill AJ, Heater KJ, Agrawal CM. The effects of physical aging in polycarbonate. J Polym Sci, Part B: Polym Phys 1990;28(3):387–405.

[33] Struik LC. Orientation effects and cooling stresses in amorphous polymers. Polym Eng Sci 1978;18(10):799–811.